



# Therapeutic potential of luteolin-loaded poly(lactic-co-glycolic acid)/modified magnesium hydroxide microsphere in functional thermosensitive hydrogel for treating neuropathic pain

So-Yeon Park<sup>1,2\*</sup>, Joon Hyuk Jung<sup>3\*</sup> , Da-Seul Kim<sup>1,4</sup>,  
Jun-Kyu Lee<sup>1</sup>, Byeong Gwan Song<sup>3</sup>, Hae Eun Shin<sup>3</sup>, Ji-Won Jung<sup>1</sup>,  
Seung-Woon Baek<sup>1</sup>, Seungkwon You<sup>2</sup>, Inbo Han<sup>5</sup>  
and Dong Keun Han<sup>1</sup> 

## Abstract

Neuropathic pain (NP) is a debilitating condition stemming from damage to the somatosensory system frequently caused by nerve injuries or lesions. While existing treatments are widely employed, they often lead to side effects and lack specificity. This study aimed to alleviate NP by developing an innovative sustained-release thermosensitive hydrogel system. The system incorporates hyaluronic acid (HA)/Pluronic F127 injectable hydrogel and bupivacaine (Bup, B) in combination with poly(lactic-co-glycolic acid; PLGA)/modified magnesium hydroxide (MH)/luteolin (Lut; PML) microspheres (PML@B/Gel). The PML@B/Gel was designed for localized and prolonged co-delivery of Bup and Lut as an anesthetic and anti-inflammatory agent, respectively. Our studies demonstrated that PML@B/Gel had exceptional biocompatibility, anti-inflammatory, and antioxidant properties. In addition, it exhibited efficient pain relief in in vitro cellular assays. Moreover, this functional hydrogel showed substantial sustained drug release while diminishing microglial activation. Consequently, it effectively mitigated mechanical allodynia and thermal hyperalgesia in in vivo rat models of chronic constriction injury (CCI). Based on our research findings, PML@B/Gel emerges as a promising therapeutic approach for the protracted treatment of NP.

## Keywords

Hyaluronic acid, Pluronic F127, PLGA microsphere, luteolin, bupivacaine

Date received: 22 October 2023; accepted: 27 December 2023

<sup>1</sup>Department of Biomedical Science, CHA University, Bundang-gu, Seongnam-si, Gyeonggi-do, Korea

<sup>2</sup>Division of Biotechnology, College of Life Sciences and Biotechnology, Korea University, Seongbuk-gu, Seoul, Korea

<sup>3</sup>Department of Life Science, CHA University School of Medicine, Seongnam-si, Gyeonggi-do, Korea

<sup>4</sup>Division of Engineering in Medicine, Department of Medicine, Harvard Medical School, Brigham and Women's Hospital, Cambridge, MA, USA

<sup>5</sup>Department of Neurosurgery, CHA University School of Medicine, CHA Bundang Medical Center, Seongnam-si, Gyeonggi-do, Korea

\*These authors contributed equally to this work.

## Corresponding authors:

Seungkwon You, Division of Biotechnology, College of Life Sciences and Biotechnology, Korea University, Seongbuk-gu, Seoul 02841, Korea.

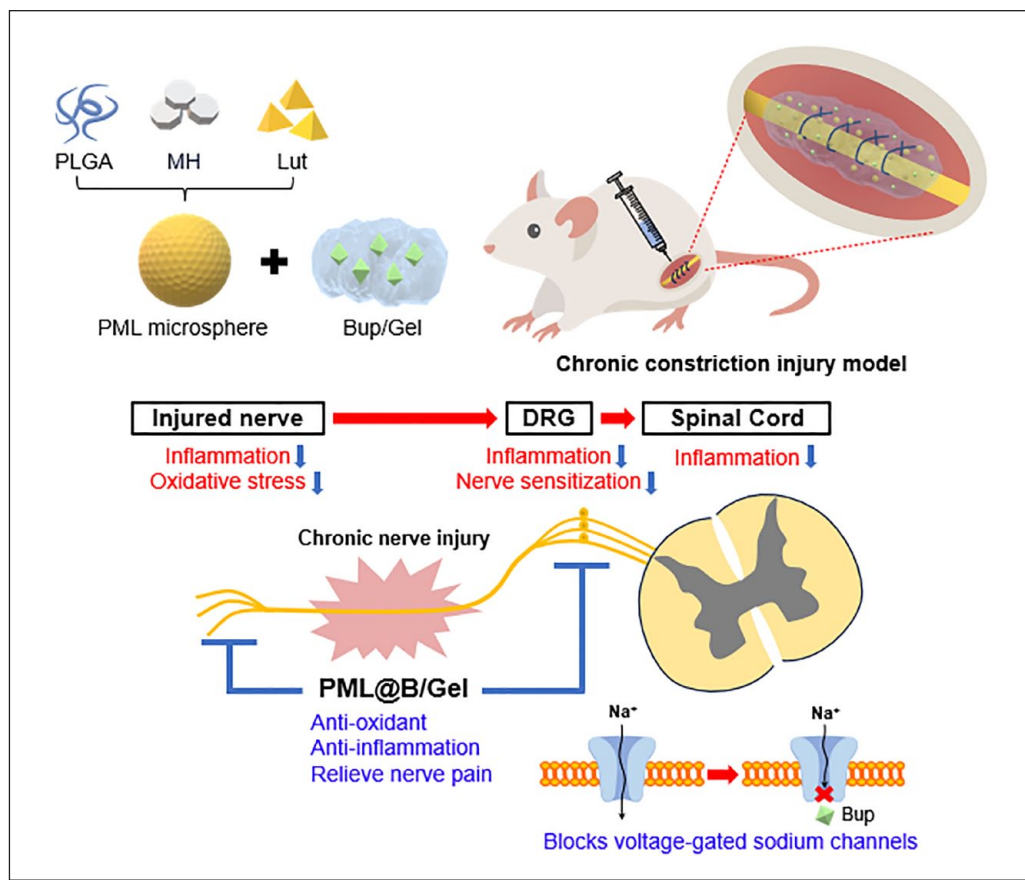
Email: bioseung@korea.ac.kr

Inbo Han, Department of Neurosurgery, CHA University School of Medicine, CHA Bundang Medical Center, 59 Yatapro, Seongnam-si, Gyeonggi-do 13496, Korea.

Email: hanib@cha.ac.kr

Dong Keun Han, Department of Biomedical Science, CHA University, 335 Pangyo-ro, Bundang-gu, Seongnam-si, Gyeonggi-do 13488, Korea.  
Email: dkhan@cha.ac.kr





**Scheme 1.** Schematic illustration of analgesic and anti-inflammatory effects of PML@B/Gel in CCI model. HA: hyaluronic acid, F127: pluronic F127, Bup: bupivacaine PLGA (P): poly(lactic-co-glycolic acid), MH (M): modified magnesium hydroxide, Lut (L): luteolin, Gel: HA/F127, DRG: dorsal root ganglion.

## Introduction

Neuropathic pain (NP) is characterized as “pain resulting from damage or disease to the somatosensory nervous system,” stemming from factors like nerve compression, pathological changes, and autoimmune diseases.<sup>1,2</sup> Globally, approximately 7%–10% of the population endures NP, leading to significant physical and psychological distress.<sup>3,4</sup> The primary pathological mechanisms of NP mainly involve central and peripheral nerve sensitization, inflammation, oxidative stress, and release of pro-inflammatory cytokines.<sup>5–8</sup> Activated microglia and macrophages contribute to the production of interleukins and tumor necrosis factor- $\alpha$  (TNF- $\alpha$ ), culminating in inflammation and cellular apoptosis. However, current therapeutic approaches, such as non-steroidal anti-inflammatory drugs (NSAIDs) and opioids, suffer from limited specificity and are associated with a wide range of side effects, including nausea, constipation, gastric and intestinal ulcers, bleeding, and perforation.<sup>9</sup>

In clinical practice, the primary approach for the initial NP treatment involves combining local anesthetics (LA) with anti-inflammatory drugs. LA function by blocking

nerve impulse transmission, thereby relieving nociceptive and/or NP. Bupivacaine (Bup), known for its prolonged duration of action, is the most commonly used LA. Dexamethasone (Dex) has shown a significant reduction in early pro-inflammatory cytokine expression when administered systemically at high doses or locally with anesthetic drugs. However, long-term and high-dose Dex administration carries various side effects, such as diabetes, glaucoma, and osteoporosis. As a result, numerous studies are exploring alternative approaches to Dex administration approaches.<sup>10–12</sup>

Luteolin (3',4',5,7-tetrahydroxyflavone, Lut) is a natural flavonoid found in edible plants, renowned for its notable anti-inflammatory and free radical-scavenging properties. Its metabolites, including luteolin glucuronide and luteolin 7-glucoside, have demonstrated various beneficial effects, encompassing antimicrobial, anti-apoptotic, anti-allergic, chemotherapeutic, and neuroprotective properties.<sup>13</sup> Despite these diverse functions, the Lut utilization is hindered by factors such as complex unsaturated structures, a short half-life, and limited water solubility. To address these challenges, we encapsulated Lut within microspheres composed of poly(lactic-co-glycolic acid);

PLGA)/magnesium hydroxide modified with ricinoleic acid (MH) using the oil-in-water method (o/w method),<sup>14</sup> improving bioavailability and facilitating targeted delivery.<sup>15</sup> However, direct injection of PLGA/MH/Lut (PML) microspheres may require an additional carrier to mitigate the risk of rapid particle dispersion within the body.

Extended-release drug delivery systems have gained considerable attention as they address essential needs in clinical pain management.<sup>16</sup> Among these systems, hyaluronic acid (HA)-based hydrogels have emerged as a promising platform for sustained drug release in various tissue repair applications.<sup>17,18</sup> By combining the sustained-release properties of hydrogels with microspheres, it becomes feasible to significantly extend the release duration. Pluronic F127 (F127), an FDA-approved triblock copolymer with established clinical applications, possesses a unique property of transiting to a solid gel state at body temperature while maintaining flowability at low temperatures.<sup>19</sup> Consequently, this distinctive characteristic of the dual hydrogel system makes it suitable for drug loading and composite formation, facilitating localized sustained drug release.

This study aims to design, prepare, and evaluate a sequential release system comprising HA/F127 injectable hydrogel loaded with Bup and PML microspheres (PML@B/Gel) to deliver anesthetic and anti-inflammatory agents in the model of rat chronic constriction injury (CCI).

## Materials and methods

### Preparation and characterization of PLGA-based microspheres

An oil-in-water (o/w) emulsion-solvent evaporation method was used. polyvinylalcohol (PVA) solution (2 w/v%, Mw 13,000–23,000, pH 8.5 in deionized water) was prepared for the external aqueous phase. Poly(lactico-glycolic acid; PLGA; 50:50, 110 kDa, 5 w/v%), magnesium hydroxide modified with ricinoleic acid 20 parts per hundred resin (phr), and Lut 50phr were dissolved in dichloromethane (DCM) as the internal oil phase. The mixture was sonicated for 10 min, and then homogenized at 600 rpm for 1 min (L5M-A, Silverson, USA) into the aqueous phase. The PLGA, PM, and PML encapsulated microspheres were also prepared following the above process. PLGA-based emulsion was dried for 60 min to evaporate the remaining DCM at room temperature (RT). The fabricated microspheres were filtered out using a sieve to 100–200  $\mu\text{m}$  sizes. The microspheres were washed in deionized water to remove impurities. In the following step, the microspheres were lyophilized for at least 3 days and stored at  $-20^{\circ}\text{C}$ . To confirm the Lut encapsulated efficiency, the microspheres were dissolved in chloroform and dried at RT. Encapsulated efficiency was analyzed using high performance liquid chromatography (HPLC) under the following conditions: a solvent system of acetonitrile

and 0.1% formic acid in water at pH 2.8 (in a 70:30 ratio), detection wavelength at 350 nm, column temperature set to  $35^{\circ}\text{C}$ , a flow rate of 0.8 ml/min, and a total run time of 15 min. Lut encapsulation efficiency was calculated by the following formula; Lut encapsulation efficiency (%) = (Measured Lut mass of microspheres)/(Feed mass of Lut)  $\times$  100. To visualize the surface of the microspheres, a scanning electronic microscope (SEM; GENESIS-1000, Korea) was performed. And to measure the size distributions of the microspheres, Image J was used. Each material content was analyzed using thermogravimetric analysis (TGA, TGA 4000 Instrument, Perkin Elmer, USA).

### Fabrication of PML@B/Gel

The F127 powder was dissolved in phosphate-buffered saline (PBS) solution and subsequently agitated on a rocker at  $4^{\circ}\text{C}$  for one day to yield a 40% w/v F127 solution. A thermosensitive hydrogel (Gel) was formulated by blending HA-based hydrogel (Hyundae Meditech, Korea) with a 40% w/v F127 solution in a 1:1 ratio. The Gel is simply mixed with 4% PLGA, PM, and PML microspheres to make functional hydrogel. To prepare B/Gel, an amount equivalent to 1% of Bup powder was dispersed in a PBS solution, and F127 powder was dissolved in a PBS solution in which Bup solution. The preparation procedure for this group was the same as the other groups except for the Bup solution. To avoid unintentional gelation, each component was stored at  $4^{\circ}\text{C}$ . A 100  $\mu\text{L}$  of PML@B/Gel contains 50  $\mu\text{g}$  of bupivacaine and approximately 795  $\mu\text{g}$  of luteolin in 4 mg microsphere.

### Characterization of PML@B/Gel

For characterized rheological evaluations, the hydrogels were undertaken using a stress-controlled rheometer (Anton-Paar, Graz, Austria). This was equipped with a parallel-plate geometry of 25 mm diameter. A consistent gap of 1000  $\mu\text{m}$  was maintained throughout the measurements. To characterize the hydrogel's linear viscoelastic behavior, a frequency sweep was executed, spanning a range from 0.1 to 10 Hz, at a controlled temperature of  $25^{\circ}\text{C}$ . The temperature-dependent sol-gel transition of the gel was measured in the range  $15^{\circ}\text{C}$ – $40^{\circ}\text{C}$  at  $0.5^{\circ}\text{C}$  intervals using a HAAKE<sup>TM</sup> Viscotester<sup>TM</sup> 3 rotational viscometer.

### In vitro drug release test

For the drug release test of Lut in the microsphere and Bup in Gel, a 100  $\mu\text{l}$  of functional hydrogel was injected in 1 ml of PBS solution containing Tween (T) 20 (0.5% w/v). Then, samples were incubated in a shaking water bath to mimic in vivo system. At a predetermined time, the released Lut was extracted from the solution and freeze-dried overnight in vacuum oven. Thereafter, the supplement was refilled with 0.5 ml of PBS solution containing

T20. A minimum of three trials were conducted with different degradation gel supernatants.

### *In vitro cell proliferation and biocompatibility*

Cell proliferation was evaluated using CCK-8 to conduct an equivalent efficacy of Lut and Dex. The cells were seeded in a 96-well plate at  $2.5 \times 10^3$  cells/ml and treated with various concentrations of Lut and Dex solution. After 24h treatment, the cells were washed with PBS solution, and CCK-8 solution was added to each well and incubated at 37°C for 2h. Absorbance was measured at 450 nm using a microplate reader. For the Live/Dead assay, the cells were seeded in 24 well plate at  $1.5 \times 10^4$  cells/ml and treated with the functional gel-conditioned media. A mixture of calcein-AM and EthD-1 (Live/Dead assay kits, Thermo Fisher Scientific) were incubated with the cells and incubated at 37°C for 1h. The cells were observed using fluorescence microscopy.

### *Flow cytometry analysis*

Cells were stained for 7-Aminoactinomycin D viability staining solution for 5 min at 4°C. The cells were washed with FACS buffer before incubation in fixation buffer at 4°C for 10 min, before performing the flow cytometry analysis. Finally, flow cytometry data were analyzed using CytExpert and FlowJo software.

### *Immunocytochemistry*

Cells were seeded on the coated cover glass in the 24 well plate. After treatment, cells were fixed with a 4% paraformaldehyde (PFA) solution for 15 min. Then cells were rinsed carefully with PBS solution to remove the PFA solution and permeabilized for 15 min with 0.2% Triton X-100. Following steps cells were blocked with Ready Probes™ 2.5% Normal Horse Serum (Thermo Fisher) to reduce the nonspecific background intensity for 1h. After 1h, cells were incubated with primary antibody overnight at 4°C. The next day cells were incubated with secondary antibodies for 1h at RT. After antibody labeling, the cells were washed with PBS solution and the nuclei were stained with an antifade mounting medium with DAPI (Vector Laboratories, USA). The primary antibodies included the antibody IL-1 $\beta$  and antibody. The secondary antibody was Alexa Fluor 488 donkey anti-rabbit IgG (Thermo Fisher) and Alexa Fluor 555 goat anti-mouse (Abcam, UK).

### *Quantitative real-time PCR (qRT-PCR) analysis of human neuroblastoma (SH-SY5Y) and rat sciatic nerve tissue*

The effect of the PML@B/Gel on inflammation, scavenged ROS, and pain was analyzed. The gene expression levels were assessed using qRT-PCR from neuroblastoma

and nerve tissue. The cells under the same experimental conditions as the biocompatibility test were treated with TNF- $\alpha$  (50 ng/ml) for 24h before retrieving mRNA. For mRNA isolation from nerve tissue, Trizol reagent (Invitrogen, USA) was used. Then the cDNA was synthesized by random hexamer primers and a TAKARA RT reagent kit (Takara, USA). SYBR Green Master Mix (Applied Biosystems, USA). The expression of target genes was normalized by 18S rRNA as a reference gene.

### *Measurement of free radical scavenging capacity*

To assess the antioxidant capacity of Luteolin, comprehensive evaluations were conducted employing the 2,2-diphenyl-1-picrylhydrazyl (DPPH) and 2,7-dichlorodihydrofluorescein diacetate (DCF-DA, Cayman, USA). In the DPPH assay, samples from each microsphere-hydrogel group (100  $\mu$ l) were injected into a DPPH working solution (250 mM, 400  $\mu$ l). This mixture was incubated at RT for 30 min in a light-protected environment. Subsequent spectrophotometric readings were taken at an absorbance of 515 nm using a precision microplate reader. For a more granulated understanding of the antioxidant activity, cells were incubated in conditioned media containing solubilized gel. Subsequently, on the second day, cells were exposed to a 750  $\mu$ M hydrogen peroxide solution for 3h. Following this treatment, cells were evaluated utilizing the DCF-DA. The DCF-DA was used at a concentration of 20  $\mu$ M. Cells subjected to this treatment were incubated for 45 min at 37°C under light-shielded conditions. Post-incubation, both viable cells and those exhibiting DCF-DA fluorescence were imaged utilizing a fluorescent microscope (CKX53, Olympus, Japan).

### *Animals and modeling procedures*

Experiments were performed with 10-week-old Sprague-Dawley (SD) rats (weighing 200–220 g) purchased from Koatech (Korea). Animals were acclimatized to the changed housing environment 1 week before surgery. They were housed at a humidity of 55%–65%, a temperature of  $24 \pm 3^\circ\text{C}$ , a 12h light/dark cycle, and free access to food and water. All surgical procedures and husbandry were approved by the Institutional Animal Care and Use Committee of CHA University (IACUC230018). The neuropathic pain model used the CCI model. SD rats were randomized into four groups: Native group ( $n=7$ ), Injury (Chronic constriction injury model) group ( $n=10$ ), Control (Dex/Bup in PBS solution) group ( $n=6$ ), and PML@B/Gel group ( $n=9$ ). Before surgery, rats were anesthetized with tiletamine and zolazepam (Zoletil, 50 mg/kg, intraperitoneal, Virbac Laboratories) and xylazine (Rompun, 10 mg/kg, intraperitoneal, Bayer). After exposing the right sciatic nerve, four ligations were made using 4-0 silk at



1 mm intervals until slight twitching was observed. Each group was injected with drugs immediately after injury. The Control group injected Dex/Bup in PBS solution at the lesion site, and the PML@B/Gel group injected PLGA/MH/Lut microspheres 4%@Bup 0.5%/hydrogel (100  $\mu$ l) using a syringe at the lesion site. After treatment, the wound was closed using 4-0 silk. The animals were sacrificed 28 days after the injury.

### *Assessment of mechanical allodynia*

The Von Frey test was performed to assess the response to a typically innocuous stimulus. The stimulus was an electro Von Frey, e-VF (Ugo Basile Biological Instruments, model 37000-007) to measure the movement threshold of the right hind paw. The animal was placed in a plastic observation chamber with a mesh floor and allowed 10 min of acclimatization time. Movement threshold was defined as the average force (g) required to retract the paw in three trials. Tests for mechanical allodynia were performed one day before injury and at 1, 3, 7, 14, 21, and 28 days after injury.

### *Assessment of thermal hyperalgesia*

A previously used method can be used to determine the thermal threshold in rats. Animals were placed in a hot plate (Ugo Basile Biological Instruments, model 35150-001) set at 52°C and the time to response (sec) was measured. Animals spent 10 min of acclimatization time in the plastic observation chamber. Animals were transferred to the apparatus set at 52°C and the time to respond was measured. Responses included pawing, licking, jumping, and two consecutive steps. The interval between trials was 10 min to prevent heat-induced tissue damage, and the cut-off time at 52°C was considered to be 20 s. The thermal threshold was defined as the number of seconds to respond in three trials. Tests for thermal hyperalgesia were performed one day before injury and at 1, 3, 7, 14, 21, and 28 days after injury.

### *Tissue processing*

Rats were sacrificed 28 days after surgery. Rats were anesthetized in the same manner as surgery and perfused with 0.9% saline and 4% PFA. The spinal cord (lumbar 4–5, L4–L5), dorsal root ganglion (DRG), and right sciatic nerve were harvested. The harvested tissues were fixed in 4% paraformaldehyde overnight. After fixation, they were dehydrated and paraffin-embedded to create 3  $\mu$ m tissue sections.

### *Histology (H&E)*

The sciatic nerve was fixed with 10% formalin solution (Sigma-Aldrich) for 72 h. Subsequently, the samples were

dehydrated in anhydrous ethanol. The samples were subsequently processed and prepared for paraffin embedding and sectioned into 3  $\mu$ m tissue slides following standard procedures. Samples were stained using Hematoxylin and Eosin (H&E; Abcam, UK) following the established protocol.

### *ELISA*

Whole blood was collected into heparinized tubes (365985, BD Biosciences, USA). Post-collection, the samples were centrifuged at 1000–2000 *g* for 10 min using a centrifuge at 4°C. Promptly after centrifugation, the supernatant (serum) was transferred to a sterile Eppendorf tube and preserved at 2°C–8°C throughout the experimentation. For further processing, samples were diluted and then incubated with RIPA lysis buffer for a duration of 30 min. Subsequent analysis was conducted in accordance with the manufacturer's protocol for the Rat TNF-alpha DuoSet (DY510-05, R&D Systems, USA)

### *Immunofluorescence (IF)*

Sections were deparaffinized in xylene and then hydrated in ethanol. Antigen retrieval was performed by treatment with pepsin solution (GBI Labs, #E06-50) for 10 min, followed by treatment with blocking solution (1% bovine serum albumin, BSA; Sigma, A7030) for 1 h. After blocking, transient receptor potential cation channel subfamily V member 1 (TRPV1, Alomone, ACC-030-GP), ionized calcium-binding adapter molecule1 (Iba-1, Abcam, ab5076), and neuronal nuclear protein (NeuN, Abcam, ab177487) primary antibodies were diluted in antibody diluent (GBI labs, #E09-300) and incubated overnight at 4°C. Primary antibodies were washed twice with PBS-T, followed by goat anti-guinea pig 568, donkey anti-goat Alexa 568, and donkey anti-rabbit Alexa 488 diluted in antibody diluent and incubated for 1 h at RT. After washing three times with PBS-T, the slides were counterstained with 4',6-diamidino-2-phenylindole (DAPI). After washing, cover glasses were mounted using a water-soluble fluorescent mounting medium (Dako Fluorescence Mounting Medium; Agilent, Santa Clara, #S3023). The analysis of IF was measured by a digital slide scanner (Zeiss Axio Scan Z1, Carl Zeiss), and the ROIs were randomized.

### *Statistical analysis*

All statistical analyses were executed using GraphPad Prism 9.5.1 software (GraphPad Software, USA). Data were represented as mean  $\pm$  standard error of the mean (SEM), with each experiment being conducted at least thrice. Significance levels are denoted as \*\*\**p* < 0.0001, \*\*\**p* < 0.001, \*\**p* < 0.01, and \**p* < 0.05. The statistical

evaluations were carried out employing one-way analysis of variance (ANOVA) followed by post hoc analysis utilizing the Tukey method.

## Results and discussion

### Preparation and characterization of drug-loaded microspheres

PLGA, a biodegradable polymer extensively used in pharmaceutical and medical device applications, can generate monomers and oligomers during its degradation, resulting in an acidic microenvironment with a low pH. In our previous studies, we employed the o/w method to encapsulate MH, effectively neutralizing the acidic byproducts of PLGA degradation.<sup>20</sup> Furthermore, we used evaporation to minimize the premature release of the amphiphilic Lut during emulsion drying by reducing the required time (Figure 1(a)). All experimental groups, including PLGA, PLGA/MH (PM), and PML microspheres, prepared in pH-adjusted PVA solutions, consistently exhibited smooth surfaces when observed via scanning electron microscopy (SEM; Figure 1(b)). SEM images revealed uniform and nonporous spherical structures of the microspheres. To optimize material encapsulation and maintain excellent injectability we designed the microspheres with a target size distribution with a diameter of 100–200  $\mu\text{m}$ . The size distributions of PLGA, PM, and PML microspheres were measured to be  $116.8 \pm 8.5$ ,  $118.7 \pm 9.5$ , and  $114.6 \pm 12 \mu\text{m}$  ( $n=50$ ), respectively, using Image J (Figure 1(c)). This measured size range strikes an optimal balance between material encapsulation and injectability. We evaluated the content of the encapsulated materials within the microspheres using thermogravimetric analysis, as depicted in Figure 1(d). Notably, the incorporation of additives into the microspheres led to observable shifts in both the onset temperature of thermal decomposition and the residual quantity of the substances. The thermogravimetric analysis provides valuable insights into the stability and potential release characteristics of the microspheres. To investigate the chemical and physical state of Lut, XRD and ATR-FTIR analysis were conducted for PLGA, PM, PML, and Luteolin powder. As shown in Supplemental Figure S4A), Lut displayed a few typical diffraction peaks in XRD. The pattern of amorphous PLGA polymer exhibited a broad peak at the region between  $16.2^\circ$  and  $23.1^\circ$ . In PML microsphere, only a small Lut peak was detected, indicating that Lut is distributed in small amounts between the PLGA matrix. ATR-FTIR analysis also showed the same results as XRD (Supplemental Figure S4B). When comparing PML with the group without Lut, the peak for Lut appeared smaller. Based on these results, we demonstrated that Lut was distributed on the surface of PLGA a little.

### Functional hydrogels exhibited a consistent microsphere structure and release properties

To optimize the hydrogel for appropriate thermosensitive gelation properties, we tested various concentrations of F127 and observed the outcomes (Supplemental Figure S2). Both 40% and 60% (w/v) concentrations exhibited gelation at  $37^\circ\text{C}$ , however, we selected the 40% concentration due to its superior stability and adequate fluidity. The Gel was prepared by mixing HA hydrogel with 40% F127 in a 1:1 ratio, which was subsequently combined with the previously fabricated microspheres. The Gel exhibited a porous structure, whereas the other groups displayed embedded microspheres within the hydrogel matrix (Figure 2(a)). Based on the SEM images of the functional Gels, the microspheres were uniformly distributed and retained their original shape even after incorporation.

Injectable medical devices intended for various tissues must possess adequate injectability and appropriate fluidic properties.<sup>21–23</sup> We conducted rheological assessments on the functional hydrogels containing microspheres with a focus on the storage modulus ( $G'$ ) and the loss modulus ( $G''$ ),<sup>24</sup> as presented in Figure 2(b(a1)). For all samples,  $G'$  consistently exceeded  $G''$  across the entire range of angular frequencies. Moreover, the viscosity-to-elastic modulus ratio ( $\tan \delta$ ) for all groups remained below 0.2. These rheological properties indicated that the fabricated hydrogels are suitable for injectable materials with strong elastic behavior. Also, measuring the temperature-dependent viscosity of thermosensitive gels, in the group without microspheres showed that the sol-gel transition began at  $27^\circ\text{C}$ . In contrast, in the gel containing PML microspheres, the transition occurred at  $28.5^\circ\text{C}$ . The addition of the microsphere increased transition temperature slightly. It was observed that all groups completely transitioned into the gel phase above  $30^\circ\text{C}$ . Consequently, it can be inferred that upon injection into an injury site, the gel undergoes gelation without dispersing from the injected area due to body temperature (Figure 2(c)). To confirm the sustained release capabilities of Gel *in vitro*, we evaluated the release profiles of Bup and Lut using high-performance liquid chromatography (Figure 2(d)). The loading efficiency for calculating cumulative release (%) for PML microsphere was verified in Supplemental Figure S1. As expected, Bup was rapidly released through a simple mixing method with Gel, causing in pain relief within 1 h after injection and continued to be released for 2 weeks (Supplemental Figure S3). In addition, Lut encapsulated in PM microspheres exhibited continuous release for a month, ensuring effectiveness throughout the entire NP treatment process. As PLGA decomposed, it generated acidic monomers (lactide and glycolide), which could induce tissue inflammation due to a low pH.<sup>25–27</sup> To assess the neutralization effect of MH on PLGA, we monitored

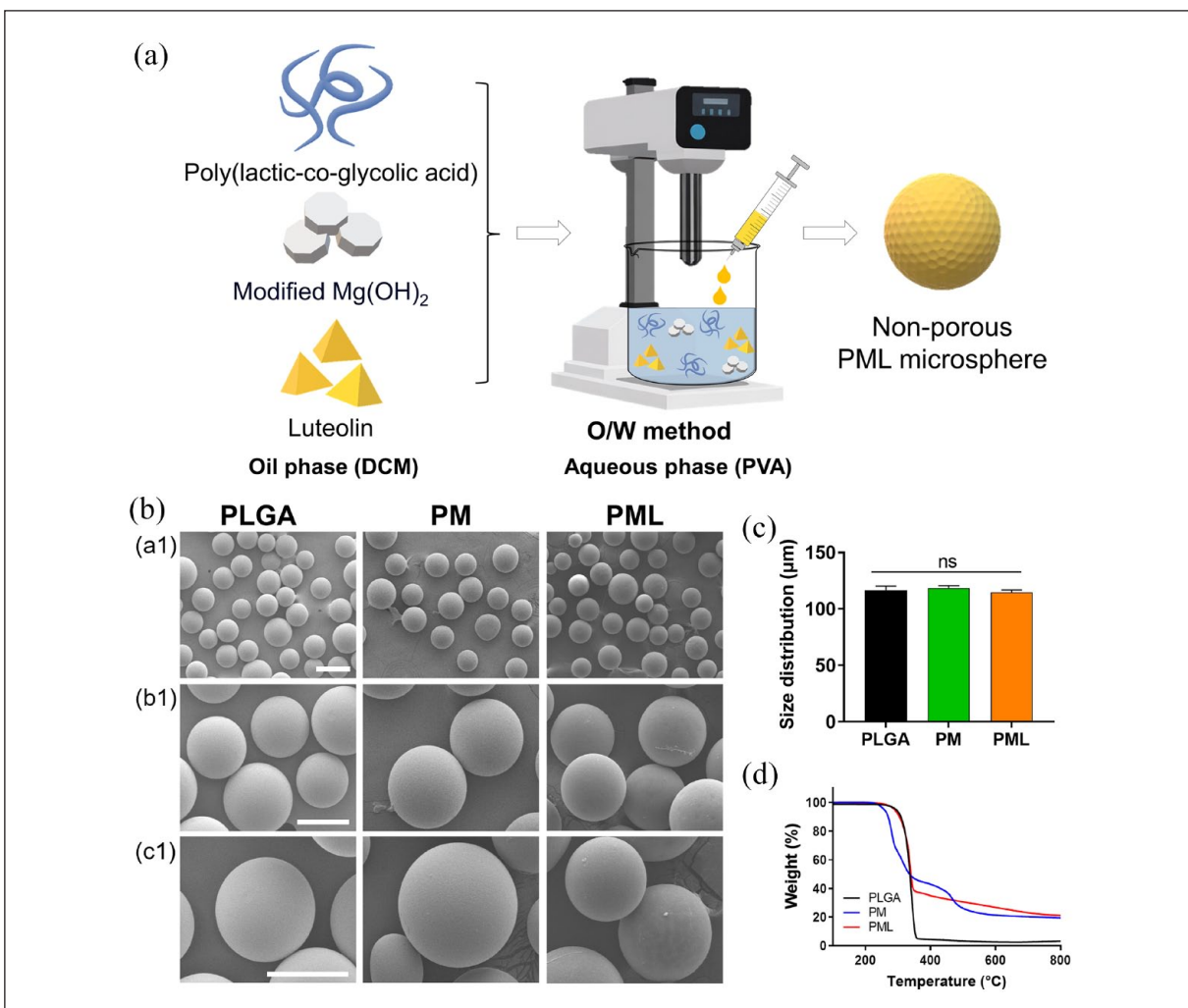


**Figure 1.** Preparation and characterization of microspheres: (a) schematic illustration of PML microsphere preparation, (b) scanning electron microscopy images of PLGA, PM, and PML microspheres (Scale bar: (a1) 200 μm, (b1, c1) 100 μm), (c) size distribution of PLGA, PM, and PML microspheres as determined by Image J, and (d) thermogravimetric analysis thermograms of PLGA, PM, and PML microspheres with varying compositions.

the pH changes of functional hydrogels during *in vitro* degradation (Figure 2(e)). While the pH of PLGA decreased to 3, the MH-containing hydrogels maintained a pH level consistent with physiological conditions. The thermosensitive hydrogel was engineered to persist for a specific period after direct delivery to the target area. Unlike typical epidural anesthetics, it can be precisely injected into localized regions, ensuring treatment at the optimal concentration at the desired site. Furthermore, its sustained release capability may reduce the need for frequent administration, thereby enhancing treatment outcomes by maintaining therapeutic effects and minimizing side effects. In conclusion, highly injectable thermosensitive hydrogels have the potential to enhance therapeutic efficacy, minimize side effects, and improve treatment outcomes through targeted and controlled release.

### Biocompatibility and anti-inflammatory effects of functional hydrogels

To assess the *in vitro* biocompatibility of PML@Gel, we employed SH-SY5Y mouse neuroblastoma cells, a widely used in neurological studies encompassing investigations into neuronal differentiation, metabolism, and functions related to neurodegenerative processes, neurotoxicity, and neuroprotection.<sup>28,29</sup> The SH-SY5Y cells were stimulated with TNF-α, and the conditioned media were used to mimic an indirect, sustained release system of the hydrogels. TNF-α is an inflammatory factor involved in apoptosis and plays a pivotal role in the TNF-mediated inflammatory pathway.<sup>30</sup> Notably, TNF-α, interleukin-1 (IL-1), and interleukin-6 (IL-6) have been predominantly associated with the development of NP.<sup>31,32</sup> These

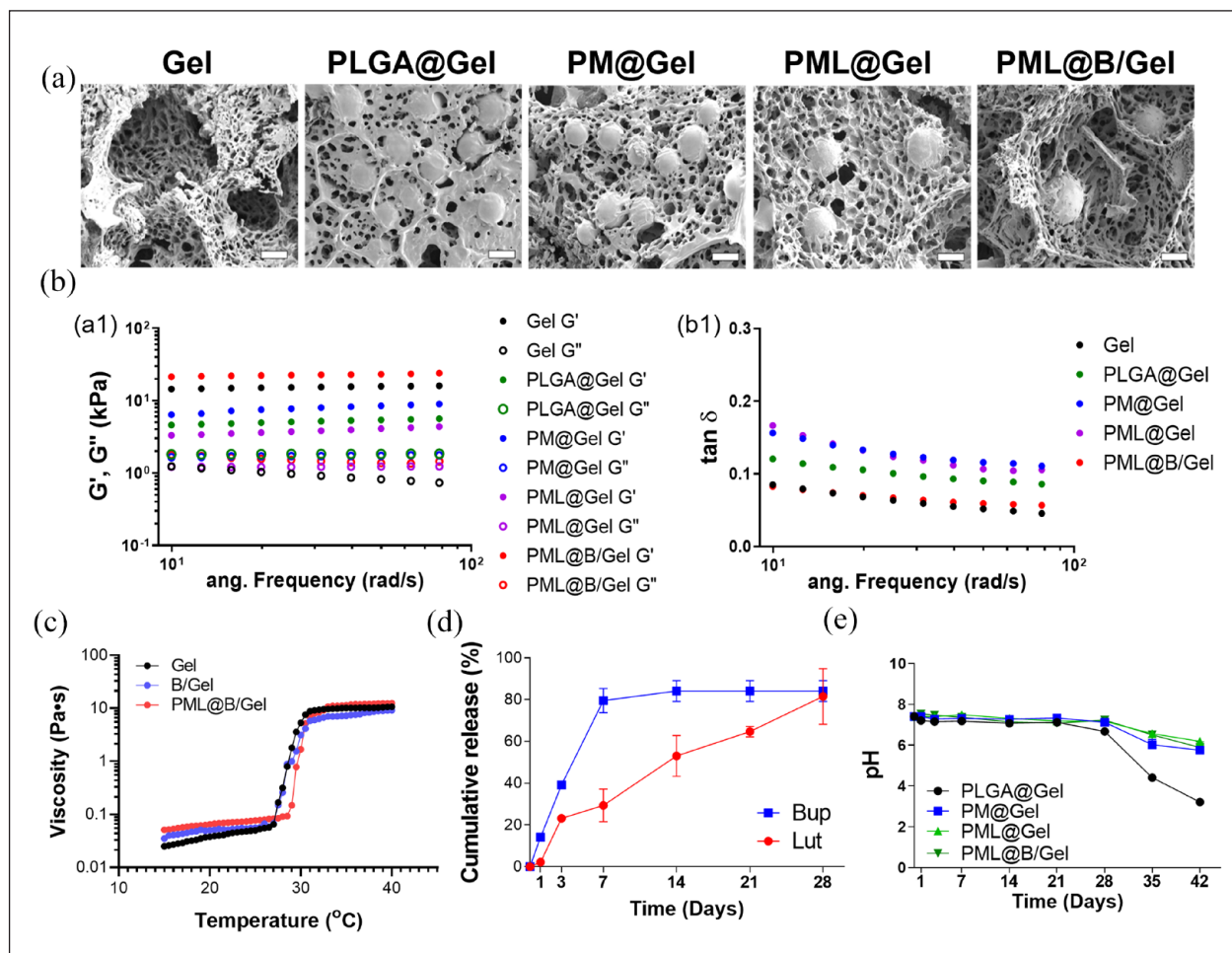


**Figure 2.** Characterization of functional hydrogels: (a) scanning electron microscopy images of the Gel, PLGA@Gel, PM@Gel, PML@Gel, and PML@B/Gel (Scale bar: 200  $\mu\text{m}$ ), (b) rheology measurement of hydrogels, (c) temperature-dependent viscosity changes of thermosensitive hydrogels from 15°C to 40°C, (d) In vitro Lut and Bup release profile for 4 weeks, and (e) pH changes of functional hydrogels during in vitro degradation behavior in PBS solution at 37°C.

well-recognized well-known cytokines exert significant roles in immunological responses and neuro-inflammatory processes, contributing substantially to the progression of chronic NP. After 24 h of TNF- $\alpha$  exposure, the viability of SH-SY5Y cells was evaluated using Live/Dead staining (Figure 3(a)) and flow cytometry analysis (Figure 3(b)). Subsequently, we evaluated the Control, TNF- $\alpha$  treated, Gel only, PLGA@Gel, PM@Gel, PML@Gel, and PML@B/Gel groups in the subsequent *in vitro* study. In comparison to the Control (TNF- $\alpha$  untreated), cell viability increased starting from the PM@Gel group with no significant difference between the Control group and the PML@Gel group. Furthermore, other studies confirmed an equivalent effect a similar effect between Lut and Dex in terms of anti-inflammation.<sup>33</sup>

We demonstrated the similar efficacy of both substances at the same concentration, suggesting the potential of Lut as an alternative to Dex (Supplemental Figure S5). In our previous research, MH-encapsulated PLGA

microspheres exhibited anti-inflammatory effects.<sup>20</sup> Lut was loaded onto the existing PM microspheres to prevent neurotoxicity and provide additional anti-inflammatory effects.<sup>34</sup> Immunocytochemistry (ICC) staining was employed to analyze IL-1 beta (IL-1 $\beta$ ), a pro-inflammatory cytokine. Compared to the control group, the expression of IL-1 $\beta$  increased following treatment with TNF- $\alpha$ . Gel groups displayed no significant difference, while the PLGA group exhibited a slight inflammatory reaction due to decomposition products. However, starting from the PM group, anti-inflammatory effects became evident, and fluorescence expression gradually decreased (Figure 3(c)). We conducted quantitative reverse transcription polymerase chain reaction (qRT-PCR) to verify the anti-inflammatory effect at the intracellular mRNA level. Consistent with the ICC staining results, the expression of inflammation-related markers, including NF- $\kappa\text{B}$ , IL-6, and COX2, decreased in the PML@Gel and PML@B/Gel groups (Figure 3(d)). The inflammatory environment,



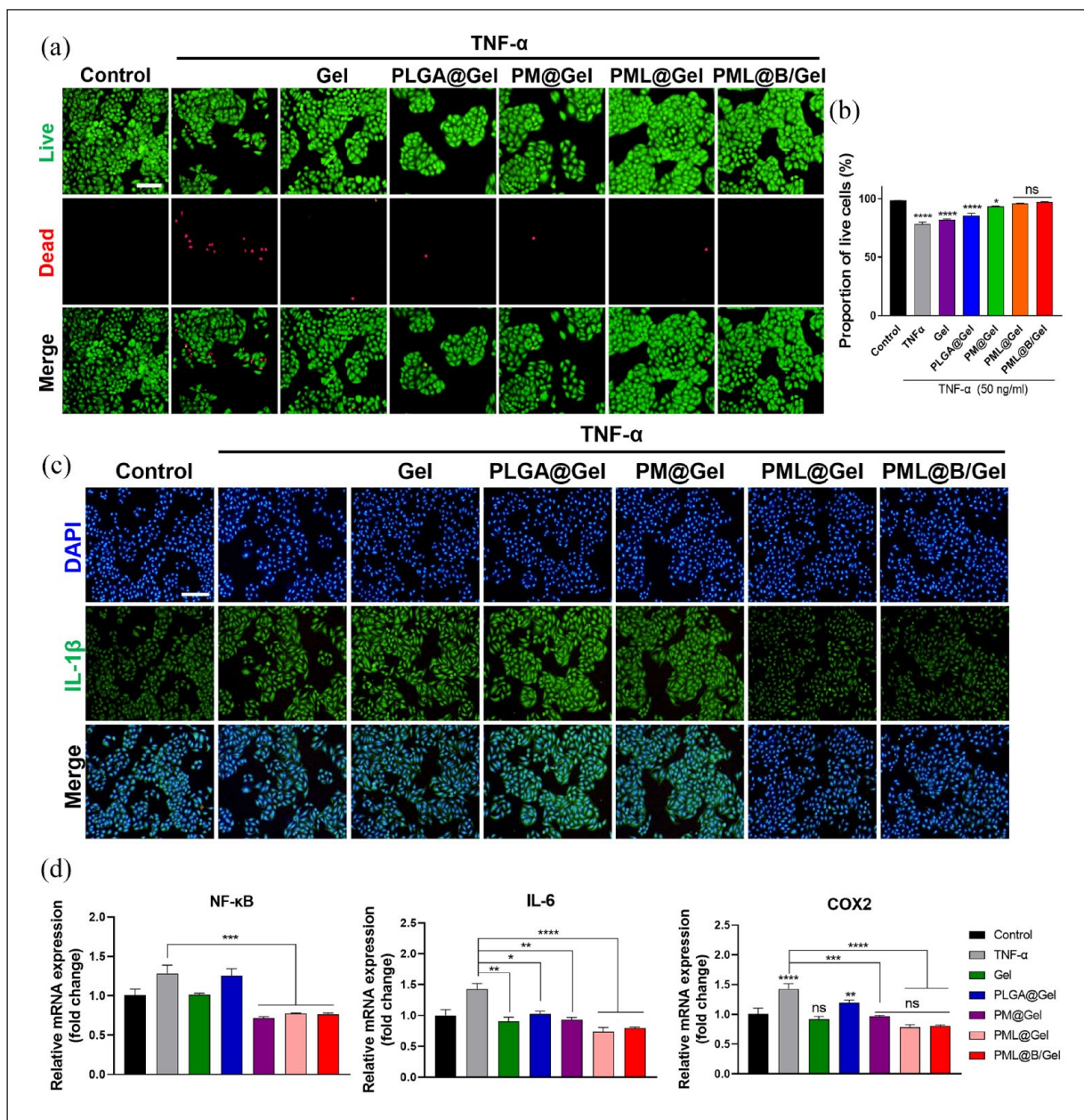


**Figure 3.** Biocompatibility and anti-inflammatory effects of functional hydrogels: (a) live/dead staining images for 24 h (Scale bar: 100  $\mu$ m), (b) flow cytometry analysis for the proportion of live cells, (c) ICC labeled with IL-1 $\beta$  antibody (Scale bar: 200  $\mu$ m), and (d) the mRNA expression levels of inflammation-related genes (NF- $\kappa$ B, IL-6, and COX2) by qRT-PCR. \*\*\*\* $p$  < 0.0001. \*\*\* $p$  < 0.001. \*\* $p$  < 0.01, and \* $p$  < 0.05 indicate statistically significant differences, respectively.

mediated by cytokines, represents a major contributor to chronic NP.<sup>35,36</sup> These findings highlight that Lut downregulates TNF- $\alpha$ , a central player in inflammation and related cellular pathways. Consequently, the restored cell viability under TNF- $\alpha$  treatment in the presence of Lut (PML@Gel and PML@B/Gel) underscores their potential therapeutic efficacy for NP. Furthermore, the comparison between Lut and the commonly used Dex reveals their comparable efficacy, suggesting that Lut is a potential alternative with fewer side effects.

### ROS scavenging of functional hydrogel effects *in vitro*

Oxidative stress results from an imbalance between excessive ROS and the antioxidant system within tissues.<sup>37,38</sup> Under normal conditions, ROS plays beneficial roles such as bactericidal action, regulation of cell division, and promotion of collagen synthesis. However, when ROS production becomes excessive, the antioxidant system's equilibrium is disrupted, leading to cell damage or cell

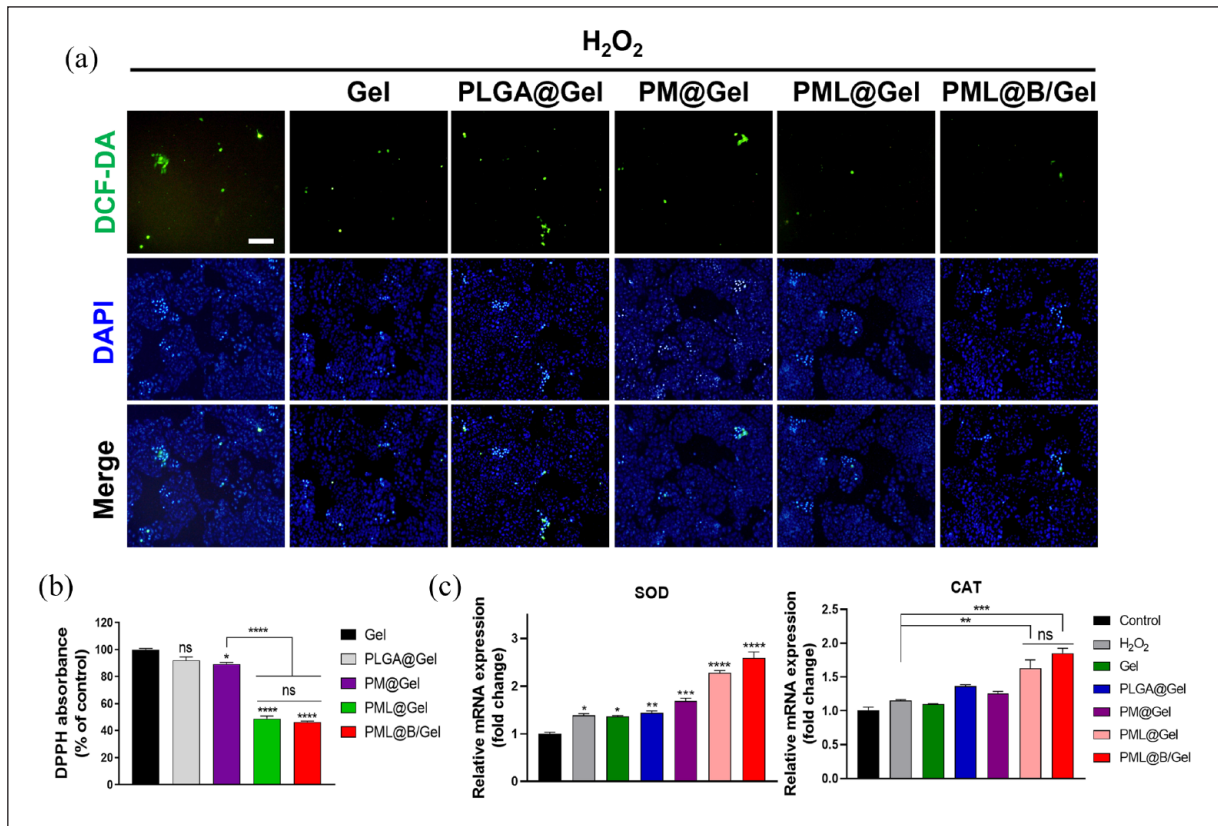


**Figure 4.** Reactive oxygen species (ROS) scavenging effects of the functional hydrogel *in vitro*: (a) fluorescence microscopy image of SH-SY5Y cells stained with DCF-DA (green) and DAPI (blue; Scale bar: 200  $\mu$ m), (b) radical scavenging activity of the hydrogel was detected using a DPPH solution, and (c) the mRNA expression levels of ROS-related genes (superoxide dismutase and catalase) by qRT-PCR.

\*\*\*\* $p < 0.0001$ . \*\*\* $p < 0.001$ . \*\* $p < 0.01$ , and \* $p < 0.05$  indicate statistically significant differences, respectively.

death.<sup>39</sup> Recent studies have demonstrated the critical role of ROS in the development of various neuropathic pains, including those arising from spinal cord injuries and extremity neuropathy.<sup>40–42</sup> Thus, we conducted functional assessments of the hydrogels to investigate their antioxidant and pain-relieving properties. The ROS-scavenging capacity of Lut in the hydrogel was assessed using DCF-DA in SH-SY5Y cells (Figure 4(a)). To replicate an environment with an excess of ROS, we optimized the H<sub>2</sub>O<sub>2</sub> dose for appropriate cell damage (Supplemental Figure S6). Relative to the group exposed to oxidative stress via H<sub>2</sub>O<sub>2</sub> treatment, the ROS-dependent fluorescence intensity was notably reduced in the PML@Gel and PML@B/Gel groups, indicating the hydrogel's antioxidant effect. In the DPPH assay, the inherent ROS activity of the materials was determined. Both Gel and PLGA@Gel showed similar results, but in comparison to the PM group, the PML@Gel and PML@B/Gel exhibited significantly reduced ROS activity (Figure 4(b)). Intracellular ROS is typically metabolized to hydrogen peroxide through the action of superoxide dismutase (SOD), which is then further reduced to H<sub>2</sub>O by catalase (CAT).<sup>43</sup> To elucidate this mechanism at the molecular level with the

hydrogel, qRT-PCR was conducted to assess mRNA expression patterns. In all groups, except for PLGA@Gel, SOD expressions were upregulated compared to the H<sub>2</sub>O<sub>2</sub>-treated group. This upregulation was particularly pronounced in the PM@Gel, PML@Gel, and PML@B/Gel groups. Additionally, while most groups did not exhibit significant variations in CAT expression, both the PML@Gel and PML@B/Gel groups displayed a notable increase in gene levels compared to the H<sub>2</sub>O<sub>2</sub>-treated group (Figure 4(c)). The presence of Lut in the PML@Gel and PML@B/Gel groups confers an antioxidant effect, as evidenced by the reduced ROS-dependent fluorescence intensity. Furthermore, Lut exhibits potential as an effective antioxidant agent, particularly in scenarios with elevated oxidative stress levels, such as the H<sub>2</sub>O<sub>2</sub>-treated group. The DPPH assay reinforces this observation by highlighting the inherent ROS activity of the materials under investigation. The upregulation in SOD expressions in most groups indicates enhanced ROS metabolism in response to the treatments, with the most pronounced enhancement observed in the PM@Gel, PML@Gel, and PML@B/Gel groups. In conclusion, based on *in vitro* analyses, the PML@B/Gel group has been identified as a superior

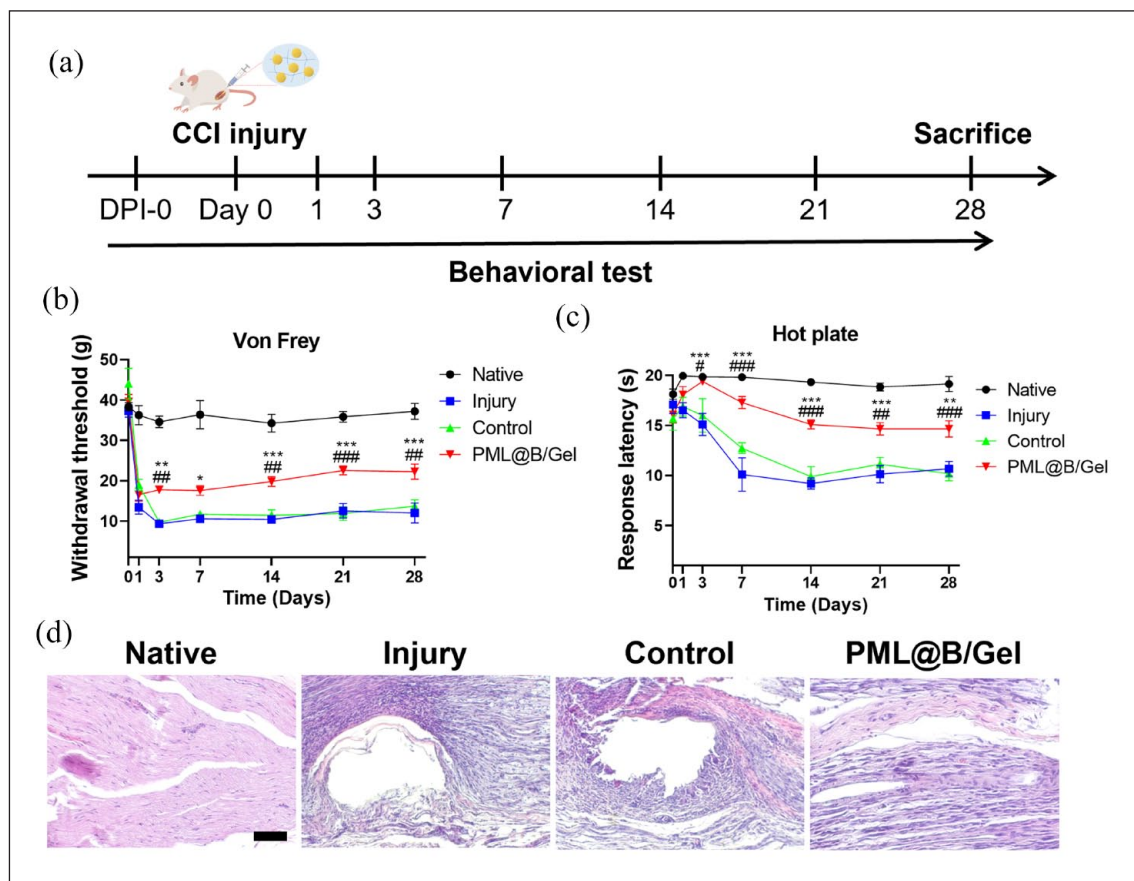


**Figure 5.** Behavioral test from DPI-0 to 28 days and histological analysis: (a) the experimental design timeline for the CCI model in rats, (b) the withdrawal threshold of the Von Frey test from the CCI surgery to 28 days post-injury is shown, and (c) the response latency of the hot plate test from CCI surgery to 28 days post-injury is shown. “\*” indicates the difference between the injury and PML@B/Gel group. “\*,” “#” indicates a significant difference with  $p < 0.05$ . “#” indicates the difference between the control and the PML@B/Gel group. “\*,” “#” indicates a significant difference at  $p < 0.05$ . “\*\*,” “##” indicates a significant difference at  $p < 0.01$ . “\*\*\*,” “###” indicates a significant difference at  $p < .001$ , and (d) H&E staining (Scale bar: 100 μm).

sustained-release hydrogel with anti-inflammatory and antioxidant properties.

### *PML@B/Gel showed a sustained effect on mechanical allodynia and thermal hyperalgesia*

The timeline for the CCI modeling and behavioral experiments spanned 28 days, as illustrated in Figure 5(a). To induce chronic peripheral NP in rats, we performed the CCI procedure on the sciatic nerves. Among the various NP symptoms induced by the injury, the primary manifestations include allodynia, characterized by pain triggered by typically non-painful stimuli, and hyperalgesia, which involved an increased pain response to typically painful stimuli.<sup>44</sup> The Von Frey and hot plate tests were employed to assess mechanical allodynia and thermal hyperalgesia, starting from one day before the surgery (DPI-0) through 28 days post-surgery (Figure 5(b) and (c)). The nerve injury resulted in a significant decrease in the withdrawal threshold (WT) when compared to Native

rats in the Von Frey test. On the first day, the WT decreased to a similarly low level in the Injury, Control, and PML@B/Gel groups. However, starting from day 3, a statistically significant difference emerged between the PML@B/Gel and the other groups ( $17.76 \pm 0.85$  g compared to below 10 g, respectively). The distinction between the PML@B/Gel and the other groups persisted throughout the entire 28-day duration.

Hot plate tests, designed to assess sensitivity to painful heat stimuli, were conducted to evaluate heat sensitivity. Initially, no differences were observed among all groups on the first day. However, starting from the third day, a significant divergence became evident in the PML@B/Gel group compared to the injured groups, with the maximum loss of response to heat occurring at 7 days in all injured rats. In contrast, the PML@B/Gel appeared to delay thermal sensation damage. In both behavioral tests, the thermosensitive hydrogel demonstrated a reduction in mechanical allodynia and thermal hyperalgesia after treatment, indicating the potential of PML@B/Gel to



effectively relieve and recover sensorimotor function loss, particularly in the early stages.

Furthermore, we conducted histological analysis to assess whether PML@B/Gel could promote the healing of the damaged sciatic nerve. Hematoxylin and Eosin (H&E) staining revealed a notable aggregation of inflammatory cells at the ligation site in the Injury and Control groups, which was distinct from the Native group (Figure 5(d)). In contrast, the PML@B/Gel group exhibited a notable reduction in the extent of the lesion caused by ligation, and tissue damage showed signs of healing. Additionally, serum ELISA analyses showed decreased TNF- $\alpha$  levels in the PML@B/Gel group. This suggests that the systemic inflammatory response triggered by CCI was mitigated following the administration of the Lut-containing hydrogel (Supplemental Figure S7). These findings indicate that PML@B/Gel not only alleviated pain but also positively impacted the healing process while reducing systemic inflammation associated with CCI.

### *Inhibition of TRPV1 by PML@B/Gel in DRG and spinal cord*

Transient receptor potential vanilloid 1 (TRPV1) plays a crucial role in nociceptive transmission and the transition from acute to chronic pain in pathological pain conditions.<sup>45,46</sup> Bup, a commonly used anesthetic for peripheral nerve injuries, has demonstrated effectiveness in reducing pain.<sup>47</sup> The anesthetic effect of Bup in the hydrogel was confirmed by assessing the expression of TRPV1 in the DRG and spinal cord. **IF** staining for TRPV1 was conducted in the DRG and spinal cord 28 days after surgery. In the DRG, the expression of TRPV1 significantly decreased in the PML@B/Gel and slightly reduced in the Control group compared to the Injury group, as depicted in Figure 6(a (a1–c1) and b (a1)). In the spinal cord, TRPV1 expression decreased in the PML@B/Gel group, reaching a level similar to that observed in the Native group (Figure 6(a (d1) and b (b1))). In contrast, the Injury and Control groups displayed the highest TRPV1 expression, especially in the dorsal horn of the spinal cord. Numerous studies have established that NP leads to an increase in the expression of inflammatory cytokines over time, with a corresponding rise in the gene expression of TRPV1, a pain marker.<sup>48,49</sup> The expression of NF- $\kappa$ B and COX2 genes serves as indicators of the inflammatory response at the injury sites (Figure 6(c (a1))). Regarding mRNA expression of inflammatory cytokines, the PML@B/Gel group exhibited reduced expression compared to the Native group, suggesting that alleviating additional inflammation may mitigate NP. Simultaneously, the results of TRPV1, NF- $\kappa$ B, and COX2 expression provide insight into the pain intensity of the CCI model arising from inflammation (Figure 6(c (b1))).

### *Inhibition of inflammation by PML@B/Gel in DRG, spinal cord, and sciatic nerve*

Following a peripheral nerve injury, an inflammatory cascade is initiated, leading to microglial invasion in areas such as the sciatic nerve, DRG, and spinal cord.<sup>50</sup> These microglia become significantly activated after CCI. The anti-inflammatory properties of Lut were validated by assessing the expression of ionized calcium-binding adapter molecule 1 (Iba-1), a well-recognized marker for microglial activation. Immunofluorescent staining of Iba-1 was conducted on the sciatic nerve (Supplemental Figure S8A), DRG, and spinal cord after 28 days post-surgery. Remarkably, the PML@B/Gel-treated group exhibited a significant reduction in Iba-1 expression across all three sites compared to both the Injury and Control groups. Particularly, the sciatic nerve, DRG, and spinal cord all displayed a significant decrease in Iba-1 intensity when quantifying the fluorescence in the PML@B/Gel group (Supplemental Figure S8B–D). After CCI, there is a surge in microglial activation across these lesion sites, which is indicative of neuronal inflammation with implications for nerve repair and regeneration. The results underscore that PML@B/Gel effectively reduces microglial activation, as evidenced by the reduced Iba-1 expression. The substantial reduction in TRPV1 expression, particularly when compared to both the Injury and Control groups, highlights the potent anti-inflammatory capabilities of PML@B/Gel. Moreover, these findings suggest that PML@B/Gel may play a crucial role in promoting nerve repair processes, expanding its potential implications beyond anti-inflammation.

### **Conclusion**

Our study underscores the potential of the PML@B/Gel system in addressing challenges associated with NP. By combining the advantages of Bup and PML microspheres within the HA/F127 hydrogel, we have developed a functional hydrogel that exhibits sustained drug release. This injectable thermosensitive functional hydrogel serves the purpose of healing damaged areas by removing ROS with Lut, containing antioxidant and anti-inflammatory ingredients, and alleviating pain through anesthetic ingredients. Leveraging its thermosensitivity, the hydrogel ensures localized treatment and continuous drug release. This approach not only reduces the need for frequent drug administrations but also alleviates the financial and time burdens on patients. Our results suggest that the application of PML@B/Gel holds promise as a powerful combination for *in situ* delivery of Lut and Bup, offering a potential long-term solution for managing NP. With its anti-inflammatory, antioxidant, and analgesic properties, this system is well-suited for future research and prospective clinical applications in the management of NP.



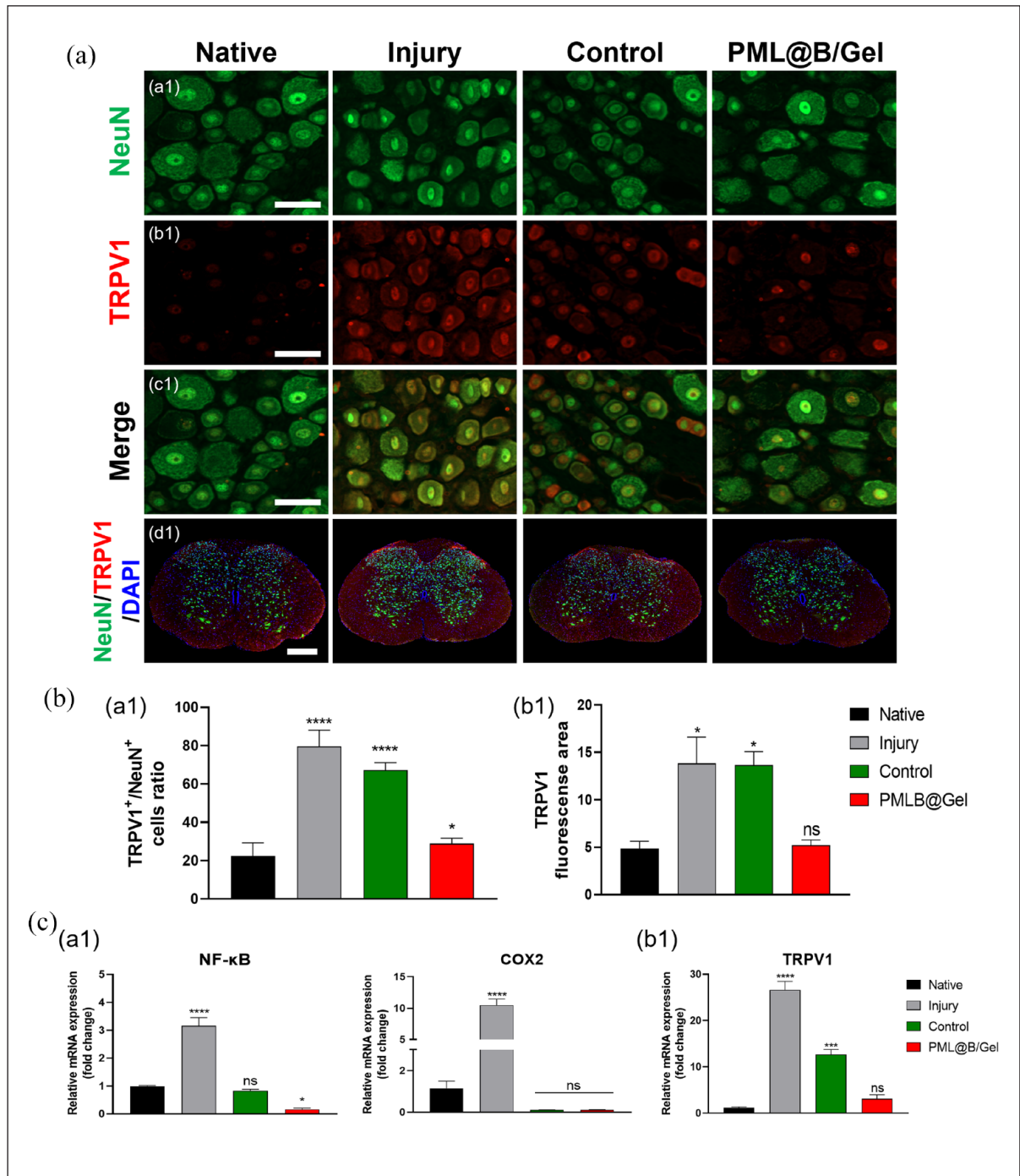


**Figure 6.** The assessment of pain receptor distribution after surgery. Immunofluorescence (IF) staining of A (a1) NeuN (green) and (b1)TRPV1 (red) in the DRG. (c1) Merged image of NeuN and TRPV1 (Scale bar: 50  $\mu$ m). (d1) IF staining of NeuN (green), TRPV1 (red) and DAPI (blue) of the spinal cord (Scale bar: 400  $\mu$ m). (b (a1)) Quantitative analysis of TRPV1<sup>+</sup>/NeuN<sup>+</sup> cells ratio in the DRG. (b1) Quantitative volumetric analysis of TRPV1 fluorescence in the dorsal horn of the spinal cord. (c (a1)) The mRNA expression levels of inflammation-related genes (NF- $\kappa$ B, COX2) and (b1) pain-related genes (TRPV1) by qRT-PCR. \*\*\*\* $p < 0.0001$ . \*\*\* $p < 0.001$ . \*\* $p < 0.01$ , and \* $p < 0.05$  indicate statistically significant differences, respectively.

## Author contributions

So-Yeon Park: Conceptualization, Writing—original draft, Validation. Joon Hyuk Jung: Conceptualization, Writing—original draft, Validation. Da-Seul Kim: Writing—review & editing, Investigation, Data curation. Jun-Kyu Lee: Writing—review & editing, Investigation. Byeong Gwan Song: Investigation, Data curation. Hae Eun Shin: Investigation, Data curation. Ji-Won Jung: Investigation, Validation. Seung-Woon Baek: Investigation, Data curation. Seungkwon You: Writing—review & editing. Inbo Han: Writing—review & editing, Super-vision. Dong Keun Han: Writing—review & editing, Super-vision, Funding acquisition.



## Declaration of conflicting interests

The author(s) declared no potential conflicts of interest with respect to the research, authorship, and/or publication of this article.

## Funding

The author(s) disclosed receipt of the following financial support for the research, authorship, and/or publication of this article: This work was supported by the Korea Medical Device Development Grant funded by the Korea Government (the Ministry of Science and ICT, the Ministry of Trade, Industry and Energy, the Ministry of Health & Welfare, the Ministry of Food and Drug Safety; Project Number: 1711196421, RS-2023-00255811); the National Research Foundation of Korea (NRF) grant funded by the Korea Government (MSIT; No. 2023R1A2C3003807); and the Korean Fund for Regenerative Medicine (KFRM) grant funded by the Korea Government (the Ministry of Science and ICT, the Ministry of Health & Welfare; 21C0717L1).

## ORCID iDs

Joon Hyuk Jung  <https://orcid.org/0009-0002-1864-4907>  
Dong Keun Han  <https://orcid.org/0000-0003-4641-7883>

## Supplemental material

Supplemental material for this article is available online.

## References

- Finnerup NB, Kuner R and Jensen TS. Neuropathic pain: from mechanisms to treatment. *Physiol Rev* 2020; 101: 259–301.
- Gangadharan V, Zheng H, Taberner FJ, et al. Neuropathic pain caused by miswiring and abnormal end organ targeting. *Nature* 2022; 606: 137–145.
- Toloui A, Ramawad HA, Gharin P, et al. The role of exercise in the alleviation of neuropathic pain following traumatic spinal cord injuries: a systematic review and meta-analysis. *Neurospine* 2023; 20: 1073–1087.
- Yu D, Mun SA, Kim SW, et al. Effects of D-serine and MK-801 on neuropathic pain and functional recovery in a rat model of spinal cord injury. *Neurospine* 2022; 19: 737–747.
- Safieh-Garabedian B, Nomikos M and Saadé N. Targeting inflammatory components in neuropathic pain: the analgesic effect of thymulin related peptide. *Neurosci Lett* 2019; 702: 61–65.
- Bhagwani A, Chopra M and Kumar H. Spinal cord injury provoked neuropathic pain and spasticity, and their GABAergic connection. *Neurospine* 2022; 19: 646–668.
- Gadot R, Smith DN, Prablek M, et al. Established and emerging therapies in acute spinal cord injury. *Neurospine* 2022; 19: 283–296.
- Lewis NE, Tabarestani TQ, Cellini BR, et al. Effect of acute physical interventions on pathophysiology and recovery after spinal cord injury: a comprehensive review of the literature. *Neurospine* 2022; 19: 671–686.
- Panchal NK and Prince Sabina E. Non-steroidal anti-inflammatory drugs (NSAIDs): a current insight into its molecular mechanism eliciting organ toxicities. *Food Chem Toxicol* 2023; 172: 113598.
- Yan L, Zhao C, Wang Y, et al. Adhesive and conductive hydrogel-based therapy simultaneously targeting neuroinflammation and neurofunctional damage after brain injury. *Nano Today* 2023; 51: 101934.
- Kong Y, Shi W, Zheng L, et al. In situ delivery of a curcumin-loaded dynamic hydrogel for the treatment of chronic peripheral neuropathy. *J Control Release* 2023; 357: 319–332.
- Ahmed YM, Orfali R, Hamad DS, et al. Sustainable release of propranolol hydrochloride laden with biconjugated-ufasomes chitosan hydrogel attenuates cisplatin-induced sciatic nerve damage in in vitro/in vivo evaluation. *Pharmaceutics* 2022; 14: 1536.
- Lopez-Lazaro M. Distribution and biological activities of the flavonoid luteolin. *Mini Rev Med Chem* 2009; 9: 31–59.
- Tian Y, Zhou J, He C, et al. The formation, stabilization and separation of oil–water emulsions: a review. *Processes* 2022; 10: 738.
- Zhang N, Lin J, Chin JS, et al. Delivery of Wnt inhibitor WIF1 via engineered polymeric microspheres promotes nerve regeneration after sciatic nerve crush. *J Tissue Eng* 2022; 13: 20417314221087417.
- Hodge JG, Zamierowski DS, Robinson JL, et al. Evaluating polymeric biomaterials to improve next generation wound dressing design. *Biomater Res* 2022; 26: 50.
- Kim DS, Kim JH, Baek SW, et al. Controlled vitamin D delivery with injectable hyaluronic acid-based hydrogel for restoration of tendinopathy. *J Tissue Eng* 2022; 13: 20417314221122089.
- Ding Y-W, Wang Z-Y, Ren Z-W, et al. Advances in modified hyaluronic acid-based hydrogels for skin wound healing. *Biomater Sci* 2022; 10: 3393–3409.
- Sanz-Horta R, Matesanz A, Gallardo A, et al. Technological advances in fibrin for tissue engineering. *J Tissue Eng* 2023; 14: 20417314231190288.
- Kim J-K, Go E-J, Ko K-W, et al. PLGA microspheres containing hydrophobically modified magnesium hydroxide particles for acid neutralization-mediated anti-inflammation. *Tissue Eng Regen Med* 2021; 18: 613–622.
- Sinclair A, O’Kelly MB, Bai T, et al. Self-healing zwitterionic microgels as a versatile platform for malleable cell constructs and injectable therapies. *Adv Mater* 2018; 30: 1803087.
- Falcone SJ and Berg RA. Crosslinked hyaluronic acid dermal fillers: a comparison of rheological properties. *J Biomed Mater Res A* 2008; 87A: 264–271.

23. Heo Y, Shin S-W, Kim D-S, et al. Bioactive PCL microspheres with enhanced biocompatibility and collagen production for functional hyaluronic acid dermal fillers. *Biomater Sci* 2022; 10: 947–959.
24. Bonany M, del-Mazo-Barbara L, Espanol M, et al. Microsphere incorporation as a strategy to tune the biological performance of bioinks. *J Tissue Eng* 2022; 13: 20417314221119895.
25. Lee J-K, Kim D-S, Park S-Y, et al. Nitric oxide-releasing bioinspired scaffold for exquisite regeneration of osteoporotic bone via regulation of homeostasis. *Adv Sci* 2023; 10: 2205336.
26. Ko K-W, Park S-Y, Lee EH, et al. Integrated bioactive scaffold with polydeoxyribonucleotide and stem-cell-derived extracellular vesicles for kidney regeneration. *ACS Nano* 2021; 15: 7575–7585.
27. Ghasemi-Mobarakeh L, Prabhakaran MP, Morshed M, et al. Application of conductive polymers, scaffolds and electrical stimulation for nerve tissue engineering. *J Tissue Eng Regen Med* 2011; 5: e17–e35.
28. Kovalevich J and Langford D. Considerations for the use of SH-SY5Y neuroblastoma cells in neurobiology. *Methods Mol Biol* 2013; 1078: 9–21.
29. Kim HN, Shin JY, Kim DY, et al. Priming mesenchymal stem cells with uric acid enhances neuroprotective properties in parkinsonian models. *J Tissue Eng* 2021; 12: 20417314211004816.
30. Xia Y, Yang R, Wang H, et al. Biomaterials delivery strategies to repair spinal cord injury by modulating macrophage phenotypes. *J Tissue Eng* 2022; 13: 20417314221143059.
31. Baka P, Escolano-Lozano F and Birklein F. Systemic inflammatory biomarkers in painful diabetic neuropathy. *J Diabetes Complicat* 2021; 35: 108017.
32. Dong J, Wang W, Zhou W, et al. Immunomodulatory biomaterials for implant-associated infections: from conventional to advanced therapeutic strategies. *Biomater Res* 2022; 26: 72.
33. Ziyang L, Yongmei Z, Nan Z, et al. Evaluation of the anti-inflammatory activity of luteolin in experimental animal models. *Planta Med* 2007; 73: 221–226.
34. Tan X-H, Zhang K-K, Xu J-T, et al. Luteolin alleviates methamphetamine-induced neurotoxicity by suppressing PI3K/Akt pathway-modulated apoptosis and autophagy in rats. *Food Chem Toxicol* 2020; 137: 111179.
35. Kuffler DP. Mechanisms for reducing neuropathic pain. *Mol Neurobiol* 2020; 57: 67–87.
36. Ramesh G, MacLean AG and Philipp MT. Cytokines and chemokines at the crossroads of neuroinflammation, neurodegeneration, and neuropathic pain. *Mediat Inflamm* 2013; 2013: 480739.
37. Olufunmilayo EO, Gerke-Duncan MB and Holsinger RMD. Oxidative stress and antioxidants in neurodegenerative disorders. *Antioxidants* 2023; 12: 517.
38. Karvandi MS, Sheikhzadeh Hesari F, Aref AR, et al. The neuroprotective effects of targeting key factors of neuronal cell death in neurodegenerative diseases: the role of ER stress, oxidative stress, and neuroinflammation. *Front Cell Neurosci* 2023; 17: 1105247.
39. Remigante A and Morabito R. Cellular and molecular mechanisms in oxidative stress-related diseases. *Int J Mol Sci* 2022; 23: 8017.
40. Kim HK, Park SK, Zhou J-L, et al. Reactive oxygen species (ROS) play an important role in a rat model of neuropathic pain. *Pain* 2004; 111: 116–124.
41. Yowtak J, Lee KY, Kim HY, et al. Reactive oxygen species contribute to neuropathic pain by reducing spinal GABA release. *Pain* 2011; 152: 844–852.
42. Choi DC, Lee JY, Lim EJ, et al. Inhibition of ROS-induced p38MAPK and ERK activation in microglia by acupuncture relieves neuropathic pain after spinal cord injury in rats. *Exp Neurol* 2012; 236: 268–282.
43. Baek S-W, Kim D-S, Lee J-K, et al. Continuous NO dual-generation by ZnO nanoparticle conjugated with  $\alpha$ -lipoic acid for functional biodegradable vascular stent. *Chem Eng J* 2023; 470: 144174.
44. Jensen TS and Finnerup NB. Allodynia and hyperalgesia in neuropathic pain: clinical manifestations and mechanisms. *Lancet Neurol* 2014; 13: 924–935.
45. Chen Y, Willcockson HH and Valtchanoff JG. Influence of the vanilloid receptor TRPV1 on the activation of spinal cord glia in mouse models of pain. *Exp Neurol* 2009; 220: 383–390.
46. Choi S-I, Lim JY, Yoo S, et al. Emerging role of spinal cord TRPV1 in pain exacerbation. *Neural Plast* 2016; 2016: 5954890.
47. Weinberg Guy L, VadeBoncouer T, Ramaraju Gopal A, et al. Pretreatment or resuscitation with a lipid infusion shifts the dose-response to bupivacaine-induced asystole in rats. *Anesthesiology* 1998; 88: 1071–1075.
48. Wang Z, Ling D, Wu C, et al. Baicalin prevents the up-regulation of TRPV1 in dorsal root ganglion and attenuates chronic neuropathic pain. *Vet Med Sci* 2020; 6: 1034–1040.
49. Xie Y-K, Luo H, Zhang S-X, et al. GPR177 in A-fiber sensory neurons drives diabetic neuropathic pain via WNT-mediated TRPV1 activation. *Sci Transl Med* 2022; 14: eab2557.
50. Coyle DE. Partial peripheral nerve injury leads to activation of astroglia and microglia which parallels the development of allodynic behavior. *Glia* 1998; 23: 75–83.